Virtual surface plasmons in cylinders

S. S. Martinos*
Department of Physics, Nuclear Research Center Demokritos, Aghia Paraskevi, Athens, Greece

E. N. Economou
Department of Physics, University of Crete, Heraklion, Crete, Greece
(Received 27 December 1982)

In a metallic cylinder virtual radiative surface eigenmodes with frequencies greater than plasma frequency exist; their dispersion curves and other properties are determined. The physical importance of these eigenmodes in the optical properties of metallic cylinders is shown.

I. INTRODUCTION

The properties of surface plasmons (SP) in cylindrical geometry (in contrast to the planar[1,2] or spherical[2,3] geometry) have received limited attention probably because of the experimental difficulties in fabricating very thin wires. Results for the dispersion relations, $\omega=\omega(k_z)$, have been obtained for real nonradiative eigenmodes in a metallic cylinder[4] assuming a simple dielectric function $\epsilon(\omega)=1-\omega_p^2/\omega^2$. Pfeiffer *et al.*[5] have studied the existence of virtual radiative eigenmodes for $\omega<\omega_p$ and have obtained the corresponding dispersion curves. Such eigenmodes have also been observed[6] experimentally. Similar calculations, including spatial dispersion, for homogeneous and inhomogeneous metallic cylinders have been done by Aers *et al.*[7] In Ref. 8 additional recent work on the optical properties of cylinders is presented.

In a previous paper[9] we examined the excitations of SP by electrons moving in circular orbits around a cylinder. Peaks in the emitted radiation for $\omega>\omega_p$, where ω_p is the bulk plasma frequency, demonstrated the existence of virtual radiative SP. In the present work we verify the existence of these virtual radiative eigenmodes and we determine their dispersion relations and other properties. Next we study the optical properties of metallic cylinders and we find that the frequencies of the eigenmodes correspond to peaks in the optical absorption spectrum. This fact shows the physical importance of the eigenmodes and points out to an easy way for their experimental observation.

A rough description of the origin of these eigenmodes and their physical meaning is as follows: Cylindrical waves are characterized by a wave number k_z along the cylinder axis (z axis) and a second "wave number" $\beta=(\epsilon\omega^2/c^2-k_z^2)^{1/2}$ along the radial direction. Here ϵ is the dielectric function of the medium and ω the frequency. If we restrict ourselves to the $k_z=0$ case, the eigenmodes of a metallic circular cylinder can be separated into transverse magnetic (TM) ones, with zero z component of the magnetic field, and transverse electric (TE) ones in which the z component of the electric field is zero. [This separation is not possible in the general case $k_z\neq 0$ (Ref. 10).] The eigenfrequencies of the TM and TE modes, respectively, are given by the equations

$$J_n(kR)H_n'(k_0R)-\sqrt{\epsilon}J_n'(kR)H_n(k_0R)=0\ , \quad (1a)$$

$$\sqrt{\epsilon}J_n(kR)H_n'(k_0R)-J_n'(kR)H_n(k_0R)=0\ , \quad (1b)$$

with $k^2=\epsilon\omega^2/c^2$, $k_0^2=\omega^2/c^2$, and R the cylinder radius. J_n and H_n are Bessel and Hankel functions of the first kind with the prime denoting differentiation with respect of the argument. If we take for the dielectric function the simple form

$$\epsilon(\omega)=1-\frac{\omega_p^2}{\omega^2} \quad (2)$$

and if we restrict ourselves to the $\omega>\omega_p$ range (where ϵ is positive and k is real) we can have a simple approximate form for Eqs. (1a) and (1b) in the limit of large R (more precisely $kR\gg 1$ and $k_0R\gg 1$). We take the square modulus of the left-hand side of Eqs. (1a) and (1b), we make use of the asymptotic forms of the Bessel functions for large arguments and we have

$$|F_n(\omega)|^2=1-\frac{\omega_p^2}{\omega^2}\sin^2\left[kR-\frac{2n+1}{4}\pi\right]=0\ , \quad (3a)$$

$$|G_n(\omega)|^2=1-\frac{\omega_p^2}{\omega^2}\cos^2\left[kR-\frac{2n+1}{4}\pi\right]=0\ . \quad (3b)$$

If we introduce for convenience the dimensionless variables $\Omega=\omega/\omega_p$ and $\alpha=R\omega_p/c$ the above equa-

tions take the form

$$|F_n(\Omega)|^2=1-\frac{1}{\Omega^2}\sin^2\left[\alpha(\Omega^2-1)^{1/2}-\frac{2n+1}{4}\pi\right]=0\,, \tag{4a}$$

$$|G_n(\Omega)|^2=1-\frac{1}{\Omega^2}\cos^2\left[\alpha(\Omega^2-1)^{1/2}-\frac{2n+1}{4}\pi\right]=0\,. \tag{4b}$$

These equations have no real roots for $\Omega>1$. But $|F_n(\Omega)|^2$ or $|G_n(\Omega)|^2$ have a minimum at the values of Ω that make $\sin^2$ or $\cos^2$ equal to unity. For those Ω's that are not much greater than unity, these minima will be close to zero and hence $|F_n(\Omega)|^{-2}$ and $|G_n(\Omega)|^{-2}$ will exhibit sharp maxima. This last condition defines a virtual eigenmode.[2] It is obvious that the eigenfrequencies correspond to values of the argument of sin and cos (and the Bessel functions) that are integral multiples of $\pi/2$. This is the condition for the creation of standing waves in the cylinder via multiple reflections. This elucidates the physical origin of these eigenmodes. Our explanation is further strengthened by the fact that the lifetime of the TM modes decreases in the vicinity of Brewster's angle as we will see in the next section.

As was mentioned above, Ω must be close to unity for the virtual eigenmodes to be well defined. We remark also that the parameter α must not be very large because in such a case the eigenmodes becomes closely spaced and almost indistinguishable. Our detailed calculations show that the surface eigenmodes with $\omega>\omega_p$ are well defined for values of Ω from 1.0 to about 1.5 and for α from about 10 to 20. This means, for a metallic cylinder, a radius of a few thousand angstroms.

In Sec. II we derive the dispersion curves $\omega=\omega(k_z)$ for the virtual eigenmodes with $\omega>\omega_p$. Their relation to the optical properties (especially optical absorption) is examined in Sec. III. Finally, in Sec. IV we present our conclusions and we discuss the properties of our eigenmodes in relation to those with $\omega<\omega_p$ and those of a metallic slab.[11]

II. VIRTUAL EIGENMODES WITH $\omega>\omega_p$

In this section we derive the dispersion curves $\omega=\omega(k_z)$ for the surface eigenmodes with $\omega>\omega_p$. Strictly speaking the dispersion curves give the real part of the complex eigenfrequency ω vs k_z. The imaginary part, which is the inverse of the mode lifetime, is given separately. We look for bound solutions of Maxwell's equations. By the term "bound" we mean solutions with no incident wave. The condition for the existence of such a solution is an equation of the general form $F(\omega,k_z)=0$. Virtual eigenmodes correspond to complex roots of this equation. Practically one looks for real values of ω that give a sharp maximum of $|F(\omega,k_z)|^{-2}$ and interprets these values as the real part of the complex eigenfrequency. The imaginary part is determined by the halfwidth of the maximum. We use this methodology in our work.

The system under consideration is a circulary cylindrical conductor of radius R in vacuum, with the cylinder axis along the z axis. The conductor is characterized by the simple dielectric function given by Eq. (2) and its magnetic permeability is supposed to be unity. The solution of Maxwell's equations[10] is a superposition of TM and TE waves of the form

$$\vec{E}_n^{(1)}=\vec{\nabla}\times\vec{\nabla}\times\vec{\Pi}_n,\quad \vec{H}_n^{(1)}=\frac{\epsilon}{c}\vec{\nabla}\times\frac{\partial\vec{\Pi}_n}{\partial t}\,, \tag{5a}$$

$$\vec{E}_n^{(2)}=-\frac{1}{c}\vec{\nabla}\times\frac{\partial\vec{\Pi}_n}{\partial t},\quad \vec{H}_n^{(2)}=\vec{\nabla}\times\vec{\nabla}\times\vec{\Pi}_n\,. \tag{5b}$$

The Hertz vector $\vec{\Pi}_n$ is

$$\vec{\Pi}_n=\hat{z}Z_n(\beta r)e^{in\theta}e^{ik_z z}e^{-i\omega t}\,, \tag{6}$$

where $\beta^2=\epsilon\omega^2/c^2-k_z^2$. The symbol Z_n stands for the proper Bessel or Hankel function of order n.

For the interior of the cylinder we have

$$\vec{E}^i=\sum_{n=-\infty}^{\infty}a_n^i\vec{E}_n^{(1)}+b_n^i\vec{E}_n^{(2)}\,, \tag{7a}$$

$$\vec{H}^i=\sum_{n=-\infty}^{\infty}a_n^i\vec{H}_n^{(1)}+b_n^i\vec{H}_n^{(2)}\,. \tag{7b}$$

We take as Z_n the Bessel function $J_n(\beta r)$ which is finite at the origin. The expressions for the exterior of the cylinder are similar to (7a) and (7b), but we take as Z_n the Hankel function of the first kind $H_n(\beta_0 r)$ with $\beta_0^2=\omega^2/c^2-k_z^2$ and the dielectric constant $\epsilon=1$. We replace also the coefficients a_n^i,b_n^i by a_n^e,b_n^e, respectively.

If we impose the well-known boundary conditions at $r=R$ we obtain for each n, the following homogeneous system:

$$-\frac{nk_z}{R}J_n(\beta R)a_n^i-\frac{i\omega\beta}{c}J_n'(\beta R)b_n^i+\frac{nk_z}{R}H_n(\beta_0 R)a_n^e+\frac{i\omega\beta_0}{c}H_n'(\beta_0 R)b_n^e=0\,, \tag{8a}$$

$$\frac{i\epsilon\beta\omega}{c}J_n'(\beta R)a_n^i-\frac{nk_z}{R}J_n(\beta R)b_n^i-\frac{i\omega\beta_0}{c}H_n'(\beta_0 R)a_n^e+\frac{nk_z}{R}H_n(\beta_0 R)b_n^e=0\,, \tag{8b}$$

$$\beta^2 J_n(\beta R)a_n^i - \beta_0^2 H_n(\beta_0 R)a_n^e = 0 , \tag{8c}$$

$$\beta^2 J_n(\beta R)b_n^i - \beta_0^2 H_n(\beta_0 R)b_n^e = 0 . \tag{8d}$$

We examine first the special case $k_z=0$. In this case, where $\beta=k=\omega\sqrt{\epsilon}/c$ and $\beta_0=k_0=\omega/c$, the above system can be separated in two subsystems: the one of Eqs. (8b) and (8c) that includes only the variables a_n^i, a_n^e and the other of Eqs. (8a) and (8d) that includes only b_n^i, b_n^e. This means a separation of the solutions of Maxwell's equations in pure TM waves [i.e., $b_n^i=b_n^e=0$ and a_n^i, a_n^e satisfying the system (8b) and (8c)] and pure TE waves [$a_n^i=a_n^e=0$ and b_n^i, b_n^e satisfying the system (8a) and (8d)]. The condition for the existence of a nontrival solution of the above subsystem is obtained by setting the determinant equal to zero. So we have the equations that give the frequencies of the TM and TE eigenmodes, respectively, for the case $k_z=0$:

$$J_n(kR)H_n'(k_0R) - \sqrt{\epsilon}J_n'(kR)H_n(k_0R) = 0 , \tag{9a}$$

$$\sqrt{\epsilon}J_n(kR)H_n'(k_0R) - J_n'(kR)H_n(k_0R) = 0 . \tag{9b}$$

If $k_z\neq 0$ we cannot make this separation. In this case the solution is a superposition of TM and TE waves and the condition for the existence of such a solution is obtained by setting the determinant of the full system (8) equal to zero:

$$\frac{\omega^2}{c^2}[\beta J_n(\beta R)H_n'(\beta_0 R) - \epsilon\beta_0 J_n'(\beta R)H_n(\beta_0 R)][\beta J_n(\beta R)H_n'(\beta_0 R) - \beta_0 J_n'(\beta R)H_n(\beta_0 R)] - \left[\frac{nk_z}{R}\right]^2 [J_n(\beta R)H_n(\beta_0 R)]^2 \frac{(\beta^2-\beta_0^2)^2}{\beta^2\beta_0^2} = 0 . \tag{10}$$

Equation (10) can be written in either of the following two forms:

$$\left[\frac{\beta}{\beta_0\sqrt{\epsilon}}J_n(\beta R)H_n'(\beta_0 R) - \sqrt{\epsilon}J_n'(\beta R)H_n(\beta_0 R)\right] - \left[\frac{nk_z}{R}\right]^2 \frac{(\beta^2-\beta_0^2)^2}{\beta^2\beta_0^2} \times \frac{c^2}{\omega^2\beta_0\sqrt{\epsilon}} \frac{[J_n(\beta R)H_n(\beta_0 R)]^2}{\beta J_n(\beta R)H_n'(\beta_0 R) - \beta_0 J_n'(\beta R)H_n(\beta_0 R)} = 0 , \tag{11a}$$

$$\left[\frac{\beta}{\beta_0}J_n(\beta R)H_n'(\beta_0 R) - J_n'(\beta R)H_n(\beta_0 R)\right] - \left[\frac{nk_z}{R}\right]^2 \frac{\beta^2-\beta_0^2}{\beta^2\beta_0^2}\frac{c^2}{\omega^2\beta_0} \times \frac{[J_n(\beta R)H_n(\beta_0 R)]^2}{\beta J_n(\beta R)H_n'(\beta_0 R) - \epsilon\beta_0 J_n'(\beta R)H_n(\beta_0 R)} = 0 . \tag{11b}$$

Equations (11a) and (11b) have the general form

$$F_n(\omega,k_z) = A_n(\omega,k_z) - k_z^2 \frac{C_n(\omega,k_z)}{B_n(\omega,k_z)} = 0 , \tag{12a}$$

$$G_n(\omega,k_z) = B_n(\omega,k_z) - k_z^2 \frac{C_n(\omega,k_z)}{A_n(\omega,k_z)} = 0 , \tag{12b}$$

and coincide with (9a) and (9b), respectively, for $k_z=0$. As was mentioned above virtual eigenmodes correspond to sharp maxima of $|F_n(\omega,k_z)|^{-2}$ or $|G_n(\omega,k_z)|^{-2}$. For $k_z=0$ these eigenmodes are pure TM or TE. If, however, $k_z\neq 0$ but it is small, the second terms in (12a) and (12b) are not so important and this separation can be extended for these values of k_z. One could make use of the terms "TM-like" and "TE-like" eigenmodes for small values of k_z with the corresponding dispersion relations $\omega=\omega(k_z)$ deriving from the maxima of $|F_n(\omega,k_z)|^{-2}$ and $|G_n(\omega,k_z)|^{-2}$, respectively. This nomenclature becomes meaningless as k_z becomes large. Nevertheless, these two branches of the dispersion relations tend to coincide as k_z becomes larger and larger as is shown from our explicit calculations.

It is convenient to insert the dimensionless variables $\Omega=\omega/\omega_p$, $\alpha=R\omega_p/c$, $q=k_z c/\omega_p$, $\lambda_0=(\Omega^2-q^2)^{1/2}$, and $\lambda=(\epsilon\Omega^2-q^2)^{1/2}$. The functions $F_n(\omega,k_z)$ and $G_n(\omega,k_z)$ can then be written

$$F_n(\Omega,q) = \left[\frac{\lambda}{\lambda_0\sqrt{\epsilon}}J_n(\lambda\alpha)H_n'(\lambda_0\alpha) - \sqrt{\epsilon}J_n'(\lambda\alpha)H_n(\lambda_0\alpha)\right] - \frac{n^2q^2}{\alpha^2\sqrt{\epsilon}\Omega^2(\Omega^2-q^2)^2(\epsilon\Omega^2-q^2)} \frac{[J_n(\lambda\alpha)H_n(\lambda_0\alpha)]^2}{\frac{\lambda}{\lambda_0}J_n(\lambda\alpha)H_n'(\lambda_0\alpha) - J_n'(\lambda\alpha)H_n(\lambda_0\alpha)} ,$$

$$G_n(\Omega,q)=\left[\frac{\lambda}{\lambda_0}J_n(\lambda\alpha)H_n'(\lambda_0\alpha)-J_n'(\lambda\alpha)H_n(\lambda_0\alpha)\right] - \frac{n^2q^2}{\alpha^2\sqrt{\epsilon}\Omega^2(\Omega^2-q^2)^2(\epsilon\Omega^2-q^2)} \frac{[J_n(\lambda\alpha)H_n(\lambda_0\alpha)]^2}{\frac{\lambda}{\lambda_0\sqrt{\epsilon}}J_n(\lambda\alpha)H_n'(\lambda_0\alpha)-\sqrt{\epsilon}J_n'(\lambda\alpha)H_n(\lambda_0\alpha)},$$

and the dielectric function becomes

$$\epsilon(\Omega)=1-\frac{1}{\Omega^2}. \tag{13}$$

In Fig. 1 we plot the real and imaginary part of the complex eigenfrequency versus q for TM-like modes and for $\alpha=10$. We mention that for each n there is a series of curves with increasing frequency and that we have plotted only the lowest one. In the higher ones the imaginary part becomes relatively large and the corresponding eigenmodes are not well defined. Figure 2 is the same as Fig. 1 but for $\alpha=15$. An interesting remark in Figs. 1(b) and 2(b) is that a maximum appears in the imaginary part of Ω at a certain value of q. To this value of q corresponds a value of $\mathrm{Re}\Omega$ via the dispersion curves of Figs. 1(a) and 1(b). These (Ω,q) pairs correspond to points on the (Ω,q) plane as shown in Fig. 3; we see that these points are very close to the curve that represents the Brewster's angle. By the term Brewster's angle we mean here the angle φ that satisfies the relation

$$\tan^2\varphi=\frac{k_z^2}{\omega^2/c^2-k_z^2}=\epsilon$$

or

$$\Omega^2=\tfrac{1}{2}+q^2+(\tfrac{1}{4}+q^4)^{1/2}.$$

The points (Ω,q) of the $\alpha=15$ case are closer to the Brewster's angle curve than those of the case $\alpha=10$. This happens because by increasing the cylinder radius we approach the plane geometry. The fact that the TM-like modes lifetime (that is the inverse of the imaginary part of Ω) decreases in the vicinity of Brewster's angle is in agreement with the physical interpretation given in the preceding section. It is well known that the reflection of TM waves is impeded at the Brewster's angle.

In Fig. 4 we show the dispersion curves for the TE-like modes and for $\alpha=10$. There are two groups of curves (dashed and solids) with some differences between them. One difference is that the first group

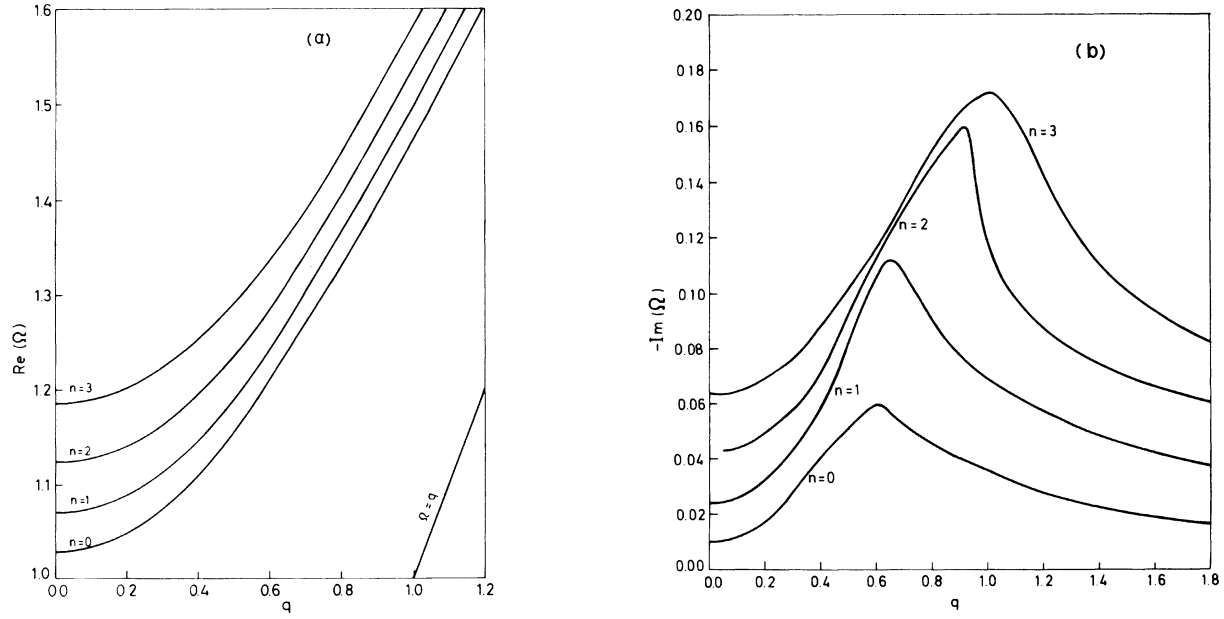

FIG. 1. (a) Dispersion curves for TM-like eigenmodes of a metallic cylinder with radius corresponding to $\alpha=R\omega_p/c=10$. There is a series of curves for each n and only the first of them is shown here. (b) The imaginary part of the complex eigenfrequency vs q (i.e., the inverse of the mode lifetime). There is a maximum in the imaginary part that corresponds to Brewster's angle.

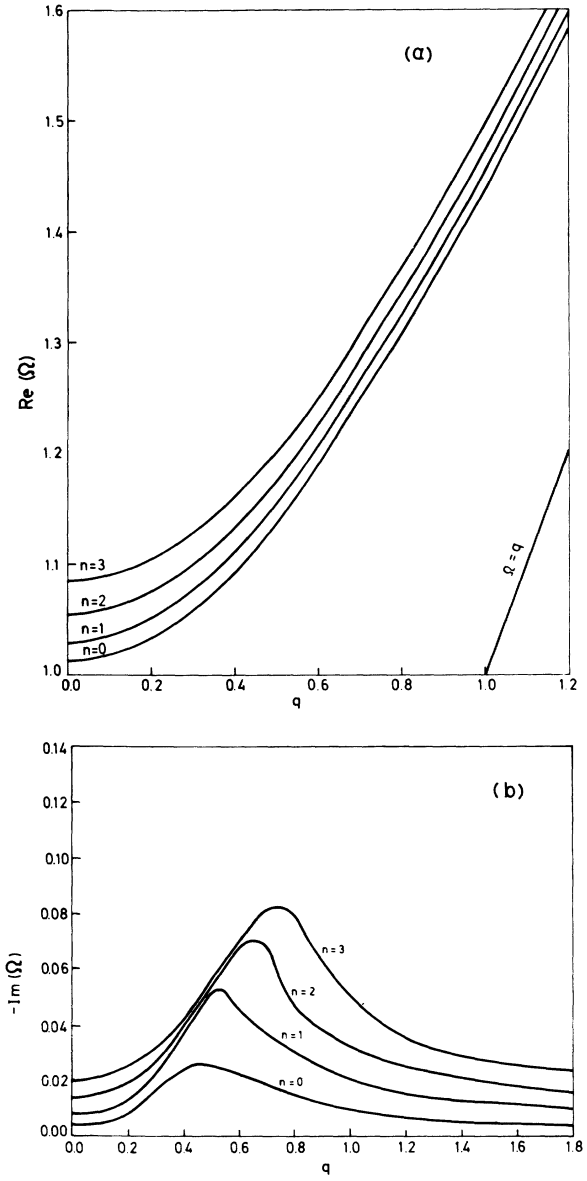

FIG. 2. Same as Fig. 1 but for $\alpha=15$.

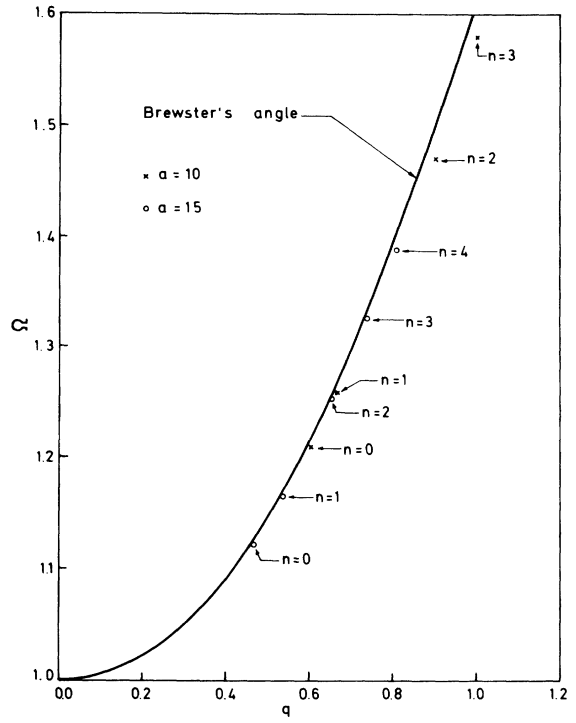

FIG. 3. Positions of maximum of the imaginary part of the complex eigenfrequency of TM-like modes for $\alpha=10$ and 15. The curve relates the frequency Ω and the wave number q corresponding to the Brewster's angle.

(a) does not contain the $n=0$ mode. We have also different behavior in the imaginary part, where the modes of the first group exhibits a maximum unrelated with the Brewster's angle.

In both TM- and TE-like eigenmodes the dispersion curves $\mathrm{Re}\Omega=f(q)$ approach the photon line $\Omega=q$ (i.e., $\omega=ck_z$) as q increases. Also the curves of the two types tend to coincide as q increases. With increasing q the eigenfrequency increases and the dielectric function $\epsilon\rightarrow 1$. In this case, as we can see from Eqs. (11a) and (11b) $F_n(\Omega,q)\rightarrow G_n(\Omega,q)$. We repeat that for large q the modes are superpositions of TM and TE waves and thus we cannot talk about TM- or TE-like modes.

III. OPTICAL PROPERTIES

In this section we study the interaction of electromagnetic radiation with a metallic cylinder with special emphasis on the excitation of the eigenmodes of the preceding section. We calculate the optical absorption spectrum (i.e., the absorptivity as a function of the frequency) for the case of perpendicular incidence of a plane electromagnetic wave with p or s polarization.

The general case of incidence of a plane electromagnetic (EM) wave on a cylinder is shown in Fig. 5. The cases of p and s polarization correspond to 0° and 90° for the angle ψ, respectively. For perpendicular incidence ($k_z=0$) the extinction, scattering and absorption coefficients are given by[12]

$$Q_{\mathrm{ext}}=-\frac{2}{\alpha\Omega}\sum_{n=-\infty}^{\infty}\mathrm{Re}(a_n+b_n)\,, \tag{14a}$$

$$Q_{\mathrm{sca}}=\frac{2}{\alpha\Omega}\sum_{n=-\infty}^{\infty}(|a_n|^2+|b_n|^2)\,, \tag{14b}$$

$$Q_{\mathrm{abs}}=Q_{\mathrm{ext}}-Q_{\mathrm{sca}}\,. \tag{14c}$$

The terms a_n,b_n for p polarization are

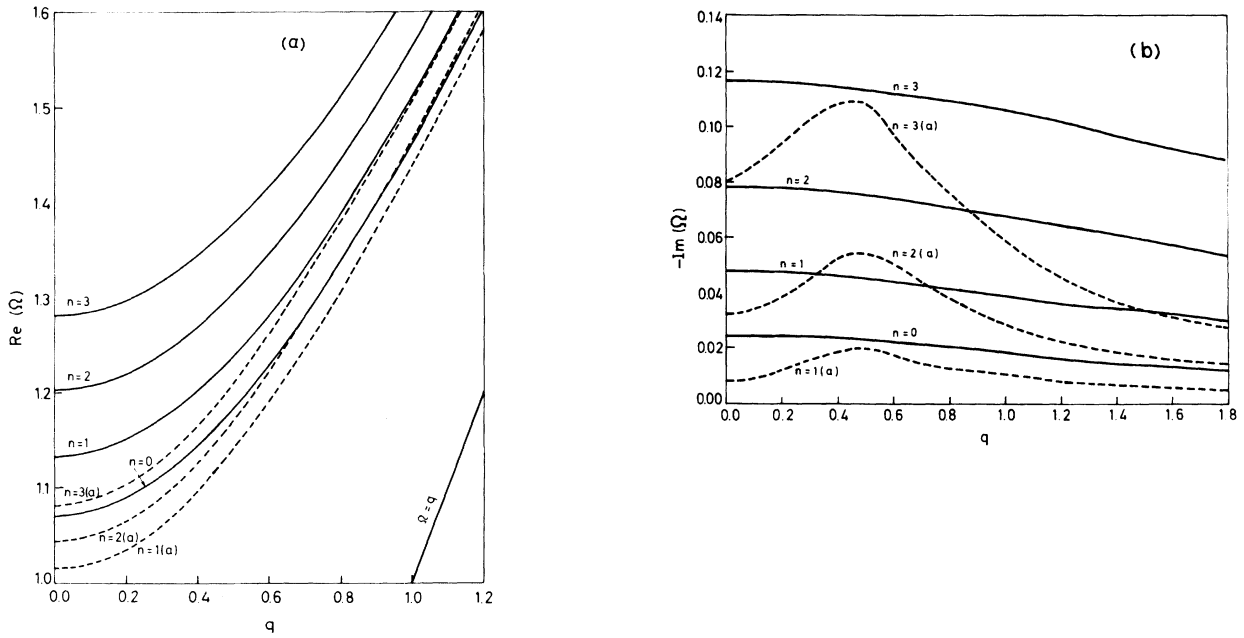

FIG. 4. (a) Dispersion curves for TE-like eigenmodes of a metallic cylinder with $\alpha=10$. Dashed and solid lines represent two different groups of eigenmodes. (b) Imaginary part of the complex eigenfrequency vs q. The maxima for the modes of the group (a) have no relation to the Brewster's angle.

$$a_n=-\frac{J_n(\alpha\Omega\sqrt{\epsilon})J_n'(\alpha\Omega)-\sqrt{\epsilon}J_n'(\alpha\Omega\sqrt{\epsilon})J_n(\alpha\Omega)}{J_n(\alpha\Omega\sqrt{\epsilon})H_n'(\alpha\Omega)-\sqrt{\epsilon}J_n'(\alpha\Omega\sqrt{\epsilon})H_n(\alpha\Omega)}\,, \tag{15a}$$

$$b_n=0\,, \tag{15b}$$

and for s polarization,

$$a_n=0\,, \tag{16a}$$

$$b_n=-\frac{\sqrt{\epsilon}J_n(\alpha\Omega\sqrt{\epsilon})J_n'(\alpha\Omega)-J_n'(\alpha\Omega\sqrt{\epsilon})J_n(\alpha\Omega)}{\sqrt{\epsilon}J_n(\alpha\Omega\sqrt{\epsilon})H_n'(\alpha\Omega)-J_n'(\alpha\Omega\sqrt{\epsilon})H_n(\alpha\Omega)}\,. \tag{16b}$$

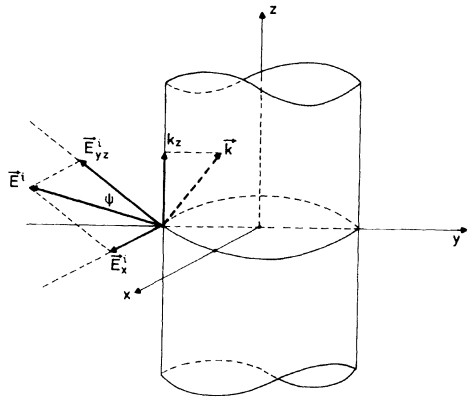

FIG. 5. Incidence of a plane electromagnetic wave of wave vector $\vec{k}$ on a cylindrical surface. The polarization is determined by the angle ψ. The magnetic field vector is not shown.

It must be pointed out[13] that the eigenfrequencies of the virtual modes with $\omega>\omega_p$ correspond to the maxima of Q_{abs} and not to the maxima of Q_{sca} or Q_{ext}. As can be seen from Eqs. (15) and (16) the eigenfrequencies minimize the denominator of Eqs. (15a) and (16b); however, at these eigenfrequencies the numerator becomes minimum as well and thus the maxima of Q_{sca} and Q_{ext} do not coincide with the eigenfrequencies. For calculating absorptivity we must, of course, take into account a damping factor in the dielectric function. Instead of the form (13) we use the form

$$\epsilon(\omega)=1-\frac{\omega_p^2}{\omega(\omega+i\tau^{-1})} \tag{17}$$

or

$$\epsilon(\Omega)=1-\frac{1}{\Omega(\Omega+i\gamma)}\ , \tag{18}$$

with $\gamma=(\omega_p\tau)^{-1}$. In numerical applications we take for the damping factor γ the typical value 0.01. From (14c) the absorption coefficient $Q_{\rm abs}$ is shown to be

$$Q_{\rm abs}=\frac{2}{\alpha\Omega}\sum_{n=-\infty}^{\infty} t_n\ . \tag{19}$$

For p polarization it is

$$t_n=\frac{2}{\pi\alpha\Omega}\frac{\mathrm{Im}[-\sqrt{\epsilon}J_n'(\alpha\Omega\sqrt{\epsilon})J_n^*(\alpha\Omega\sqrt{\epsilon})]}{|J_n(\alpha\Omega\sqrt{\epsilon})H_n'(\alpha\Omega)-\sqrt{\epsilon}J_n'(\alpha\Omega\sqrt{\epsilon})H_n(\alpha\Omega)|^2}\ , \tag{20a}$$

and for S polarization

$$t_n=\frac{2}{\pi\alpha\Omega}\frac{\mathrm{Im}[-(\sqrt{\epsilon})^*J_n'(\alpha\Omega\sqrt{\epsilon})J_n^*(\alpha\Omega\sqrt{\epsilon})]}{|\sqrt{\epsilon}J_n(\alpha\Omega\sqrt{\epsilon})H_n'(\alpha\Omega)-J_n'(\alpha\Omega\sqrt{\epsilon})H_n(\alpha\Omega)|^2} \tag{20b}$$

(the asterisk denotes complex conjugate). In Figs. 6 and 7 we plot $Q_{\rm abs}$ vs Ω for p and s polarization, respectively, and for $\alpha=10$. The peaks in these absorption spectra correspond exactly to the frequencies of TM and TE eigenmodes. We see that the sharpness of the peaks decreases with n because of the increase of the imaginary part of the eigenfrequencies. Nevertheless, the peaks for small n are clearly distinguishable and thus their experimental observation should present no major difficulty. We note that for s polarization (Fig. 7) both groups of TE-like modes are responsible for peak formation. Occasionally, due to an almost degeneracy and finite linewidth, two modes may be responsible for a single peak.

IV. CONCLUSIONS

The $\omega>\omega_p$ virtual eigenmodes studied in this work stem from a geometric resonance effect, where the "wavelength" fits the size of the circular cross section. This allows a coherent surface multiple-scattering effect to take place, which is responsible for the appearance of these virtual bound modes. As the radius of the cylinder increases (i.e., as we approach a planar geometry) the geometrical fitting becomes more precise and the virtual modes better defined. Indeed our explicit calculations show that for $\alpha\lesssim 5$ these eigenmodes cannot be defined at all. On the other hand, a very large radius makes the

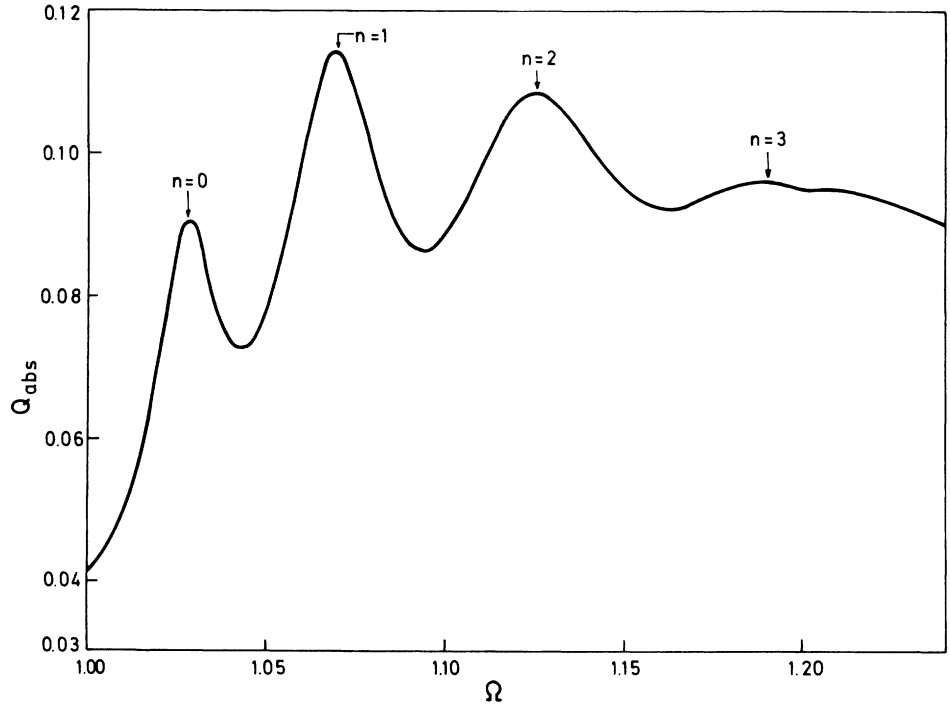

FIG. 6. Absorption coefficient $Q_{\rm abs}$ vs Ω for normal incident of a plane EM wave with p polarization. The radius of the cylinder corresponds to $\alpha=10$. The peaks for $n=0,1,2,3$ appear at the eigenfrequencies of TM modes.

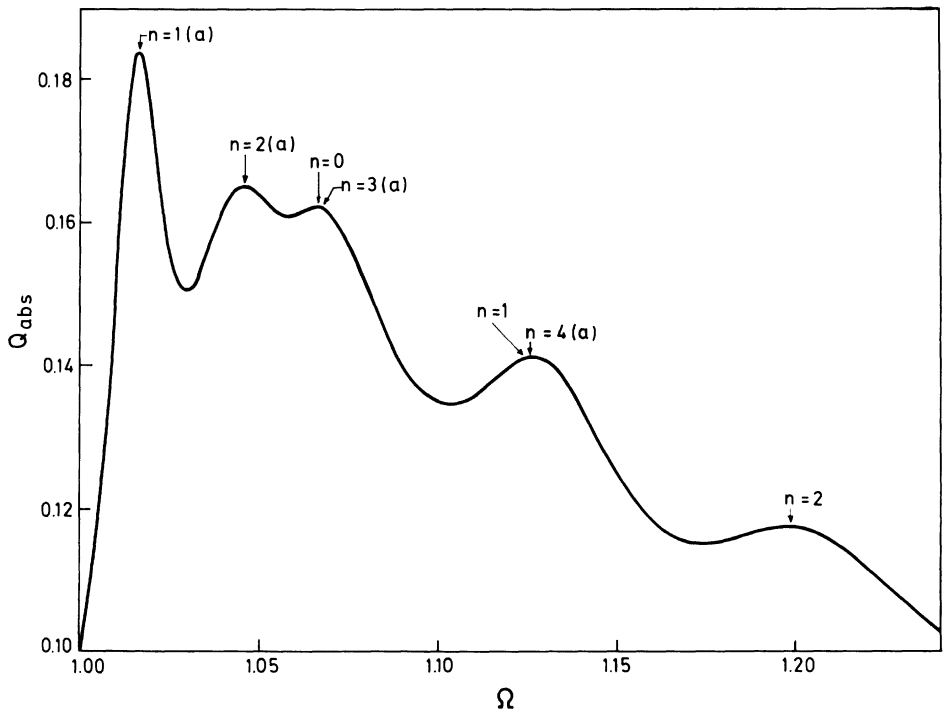

FIG. 7. Same as in Fig. 6 but for s polarization. The peaks appear now at the TE modes eigenfrequencies. Some peaks (e.g., the third and fourth ones in order of increasing frequency) are due to two almost degenerate modes.

modes so closely spaced that they become practically indistinguishable. This geometrical interpretation is consistent with our finding that the lifetime decreases with increasing n [see Figs. 1(b), 2(b), and 4(b)].

The eigenmodes of this work show many similarities with analogous eigenmodes ($\omega > \omega_p$) that exist in a metallic slab.[11] They have the same physical origin and they have a similar relation with the optical properties, i.e., the eigenfrequencies in both cases correspond to peaks in the absorption spectrum.

It is worthwhile to point out that the virtual eigenmodes with $\omega < \omega_p$ have a different (not geometrical) physical origin and exhibit a quite different behavior.[5] Their lifetime is decreasing with increasing radius α and decreasing order n.

*Present address: University of Athens, Department of Physics, Division of Mechanics, Panepistimiopolis, Athens 621, Greece.

[1]R. H. Ritchie, Phys. Rev. 106, 874 (1957); Surf. Sci. 34, 1 (1973); E. A. Stern and R. A. Ferrell, Phys. Rev. 120, 130 (1960); C. J. Powell and J. B. Swan, *ibid.* 115, 869 (1959); 116, 81 (1959); 118, 640 (1960); A. R. Melnyk and M. J. Harrison, Phys. Rev. B 2, 835 (1970); Phys. Rev. Lett. 21, 85 (1968).

[2]E. N. Economou and K. L. Ngai, Adv. Chem. Phys. 27, 265 (1974).

[3]F. Fujimoto, K. Komaki, and K. Ishida, J. Phys. Soc. Jpn. 23, 1186 (1967); F. Fujimoto and K. Komaki, *ibid.* 25, 1679 (1968); U. Kreibig and P. Zacharias, Z. Phys. 231, 128 (1970); U. Kreibig, *ibid.* 234, 307 (1970); R. H. Doremus, J. Chem. Phys. 40, 2839 (1964); J. Appl. Phys. 35, 3456 (1964); J. Chem. Phys. 42, 414 (1965); W. T. Doyle, Proc. R. Phys. Soc. London 75, 649 (1960); M. Creuzburg and H. Raether, Z. Phys. 171, 436 (1963); C. Koumelis, D. Leventouri, and K. Alexopoulos, Phys. Status Solidi B 46, K81 (1971); Th. Kokkinakis and Alexopoulos, Phys. Rev. Lett. 28, 1632 (1972); R. Ruppin, Phys. Rev. B 11, 2871 (1975).

[4]J. C. Ashley and L. C. Emerson, Surf. Sci. 41, 615 (1974).

[5]C. A. Pfeiffer, E. N. Economou, and K. L. Ngai, Phys. Rev. B 10, 3038 (1974).

[6]C. Miziumski, Phys. Lett. 40A, 187 (1972).

[7]G. C. Aers, A. D. Boardman, and B. V. Paranjape, J. Phys. F 10, 53 (1980).

[8]A. Cohen, Opt. Lett. 5, 150 (1980); V. A. Kosobukin, Fiz. Tverd. Tela Leningrad 22, 1017 (1980) [Sov. Phys.—Solid State 22, 594 (1980)]; A. B. Katrich and

V. M. Kuzmichev, Opt. Spektrosk. 48, 1126 (1980) [Opt. Spectrosc. (USSR) 48, 616 (1981)].

[9]S. S. Martinos and E. N. Economou, Phys. Rev. B 24, 6908 (1981).

[10]J. A. Stratton, *Electromagnetic Theory* (McGraw-Hill, New York, 1941).

[11]K. L. Kliewer and R. Fuchs, Phys. Rev. 153, 498 (1967).

[12]M. Kerker, *The Scattering of Light and Other Electromagnetic Radiation* (Academic, New York, 1969).

[13]R. Englman and R. Ruppin, J. Phys. C 1, 1515 (1968).